

Extragalactic Radio Sources and the WMAP Cold spot

Lawrence Rudnick, Shea Brown, Liliya R. Williams

Department of Astronomy, University of Minnesota, Minneapolis, MN 55455

ABSTRACT

We detect a dip of 20-30% in the surface brightness and number counts of NVSS sources smoothed to a few degrees at the location of the WMAP cold spot. The dip has structure on scales of $\sim 1^\circ$ to 10° . We suggest that the dip in extragalactic brightness and number counts and the WMAP cold spot are physically related, i.e., that the coincidence is neither a statistical anomaly nor a WMAP foreground correction problem. Since the cold spot originates from structures at modest redshifts, there is no remaining need for non-Gaussian processes at the last scattering surface of the CMB. The late integrated Sachs-Wolfe effect, already seen statistically for NVSS source counts, may thus be seen to operate on a single region for the first time. To create the magnitude and angular size of the WMAP cold spot requires a ~ 140 Mpc radius completely empty void at $z \leq 1$ along this line of sight. This is far outside the current expectations of the concordance cosmology, and adds to the anomalies seen in the CMB.

Subject headings: large-scale structure of the universe – cosmic microwave background – radio continuum: galaxies

1. Introduction

The detection of an extreme “cold spot” (Vielva et al. 2004) in the foreground-corrected WMAP images was an exciting but unexpected finding. At 4° resolution, Cruz et al. (2005) determine an amplitude of $-73 \mu\text{K}$, which reduces to $-20 \mu\text{K}$ at $\sim 10^\circ$ scales (Cruz et al. 2007). The non-gaussianity of this extreme region has been scrutinized, (Cayon, Jun & Treaster 2005; Cruz et al. 2005, 2006, 2007) concluding that it cannot be explained by either foreground correction problems or the normal Gaussian fluctuations of the CMB. Thus, the cold spot seems to require a distinct origin.

Most proposals about the origin of the cold spot address the radiation at the last scattering surface of the CMB. At the same time, fluctuations in WMAP images of the CMB are seen to be correlated with local mass tracers (Pietrobon, Balbi & Marinucci 2006; Cabre et al.

2006) such as the optical Sloan Digital Sky Survey (SDSS, York et al. 2000) and the radio NRAO VLA Sky Survey (NVSS, Condon et al. 1998), probably through the late integrated Sachs-Wolfe effect (ISW, Crittenden & Turok 1996). McEwen et al. (2006) took this a step further by using a wavelet analysis and isolating 18 regions that as a group, contributed a significant fraction of the NVSS ISW signature. One of their regions (#16) is close to the WMAP cold spot, the subject of this paper.

The NVSS 21 cm survey covers the sky above a declination of -40° at a resolution of $45''$. It has an rms noise of 0.45 mJy/beam and is accompanied by a catalog of sources stronger than 2.5 mJy/beam. Because of the short interferometric observations that went into its construction, the survey is insensitive to diffuse sources greater than about $15'$ in extent. Convolution of the NVSS images to larger beam sizes, as done here, shows the integrated surface brightness of small extragalactic sources; this is very different than what would be observed by a single dish of equivalent resolution. In the latter case, the diffuse structure of the Milky Way Galaxy, invisible to the interferometer, would dominate. The 408 MHz all sky map of Haslam et al. (1981) is dominated in most places by galactic emission, and is often used as a template for estimating or masking the synchrotron contribution in CMB observations.

2. Analysis and Statistics

We examine the dip in cm wave emission at different scale sizes, and in two different ways – average surface brightness and source number density. In the region of the WMAP cold spot, the galactic emission at 408 MHz (Haslam et al. 1981) is atypically low and smooth, and the small scale fluctuations are dominated by extragalactic sources. A clear dip of $\approx 11\%$ in brightness is seen at a resolution of 1° (Figure 1), within the 10° diameter circle indicating the position and full extent (Cruz et al. 2007) of the WMAP cold spot. We also convolved the NVSS survey to the same 1° resolution; it shows a much larger (62%) dip in the region of the cold spot. Note that although there is flux everywhere in the NVSS image, this is the “confusion” from the smoothed contribution of multiple small extragalactic sources in each beam, whereas the 408 MHz map has strong diffuse galactic emission as well, leading to a smaller fractional brightness dip.

We then convolved the NVSS image, which contains only extragalactic emission, to 3.4° , shown in Figure 2. Here, the region of the cold spot is seen to be the faintest region on the image (minimum at $l_{II}, b_{II} = 207.8^\circ, -56.3^\circ$), slightly fainter than other nearby locations. At minimum, its brightness is 14 mK below the mean, with an extent of $\approx 5^\circ$. The WMAP cold spot thus picks out a special region in the NVSS (at least within this 2500° region); we

now examine its statistical significance with regards to the entire sky.

We created a smoothed brightness version of the all sky NVSS survey by pre-convolving the images to $800''$ and then calculating the median brightness in sliding boxes 3.4° on a side. The median gives us an alternative way to assess the significance of the faint cold spot region, with less sensitivity to the smaller number of bright sources. The resulting image is shown in Figure 3 which is in galactic coordinates centered at $l_{II}=180^\circ$. The dark regions near the galactic plane are regions of the NVSS survey that were perturbed by the presence of very strong sources. Note that the galactic plane itself, which dominates the 408 MHz maps, is only detectable here between $-20^\circ < l_{II} < 90^\circ$, where an increase in the number of small sources detectable by the interferometer is found.

We examined the distribution of median brightnesses in two strips in the all sky map. The first was in the north, taking everything above a nominal galactic latitude of 30° (More precisely, we used the horizontal line in the Aitoff projection tangent to the 30° line at $l_{II}=180^\circ$.) The second was in the south, taking everything below a nominal galactic latitude of -30° , but only from $10^\circ < l_{II} < 180^\circ$, to avoid regions near the survey limit of $\delta=-40^\circ$. The minimum brightness in the cold spot region (≈ 20 mK) is equal to the lowest values seen in the 16,800 square degree area of the two strips, and is $\approx 30\%$ below the mean (Figure 4). Since the number of independent regions on the sky in our processing can be estimated as $16,800^\square / (3.4^\circ \times 3.4^\circ) = 1453$, the lowest region is expected to be at the $< 0.1\%$ level of the brightness distribution, as observed. The dip in the NVSS is thus significant in being at the extreme of the observed distribution, but it is part of that distribution, not an extreme outlier. We further note that the low end of the distribution is not Gaussian, cutting off more quickly than a Gaussian below the 2σ point. The origin of the 0.5 mK offset between the north and south is not clear, but does not affect our analysis.

We then look at the probability that this match between NVSS and WMAP is accidental, recognizing the *a posteriori* nature of our discussion. The exact number of regions with similarly low brightness is not easily quantified, because the pixel brightnesses change by $\approx 5\%$, depending on the exact smoothing method and sky projections used. However, we found ≈ 5 -10 such high galactic latitude low brightness regions within 10% of the minimum brightness. So another way to assess the probability of finding a dip at the center of the WMAP cold spot would be to say that we have 10 opportunities out of 1453, or 0.07%, to find one of them. A much more conservative estimate would be to allow a 3.4° faint region to lie anywhere in the 100^\square WMAP cold spot, in which case the probability of finding a faint region at random is $10 \text{ (potential sources)} \times \frac{100^\square}{16800^\square} = 6\%$. We conclude that the association of a dip in NVSS brightness and the WMAP cold spot is statistically real.

Our use of the smoothed brightness from the NVSS, as opposed to source counts, was

somewhat serendipitous; these smoothed data are being used as part of a search for diffuse large scale structures associated with cluster formation. The faint NVSS region can be seen at a number of resolutions, and there is probably more than one scale size present in this faint region. At resolutions of 1° , 3.4° , and 10° , we find that the dip is $\approx 70\%$, 30% and 10% of the respective mean brightness. At 10° resolution, the NVSS deficit overlaps with another faint region about 10° to the west, and the dip in brightness decreases from -14 mK (at 3.4°) to -4 mK.

To look more quantitatively at the source density in the cold spot region, we measured the density of NVSS sources (independent of their fluxes) as a function of distance from the cold spot. To improve the statistics, we identified all sources with a flux above 3.3σ (1.5 mJy), which is lower than the nominal NVSS survey limit of 2.5 mJy. More precisely, we counted as sources all those positions that had at least 5 contiguous $15''$ pixels above the 1.5 mJy threshold (using the AIPS task STFND) in the NVSS fields surrounding the WMAP cold spot. After eliminating duplicated sources in the field overlap regions, the threshold of 1.5 mJy results in $\approx 60\%$ more sources than are present in the NVSS catalog. The main problem with using a 3.3σ threshold are the occasional spurious noise peaks identified as sources. Since this will tend to reduce the signature of any lower source density in the direction of the cold spot, this is a conservative approach.

The results of this analysis are shown in Figure 5, in which we plot the cumulative number density of sources (count per unit area) as a function of their distance from the WMAP cold spot. A clear decrease in source density of $\approx 15\text{--}20\%$ is seen in the direction of the cold spot. The magnitude of the deficit decreases by a factor of 2 at a radius of $\approx 2.5^\circ$. We therefore assign a characteristic size of 5° to the deficit region, but note that several scales are probably present.

McEwen et al. (2006) performed an independent all sky analysis of NVSS source counts using wavelets, and identified eighteen isolated regions as responsible for a significant fraction of the correlation with WMAP. Of those eighteen regions, three were identified by both of their wavelet flagging techniques. One of these, number 16 is within a few degrees of the cold spot, the subject of this paper. This provides an independent confirmation of the validity of the dip in NVSS brightness and counts.

3. Foreground Corrections

Several studies have claimed that the properties of the cold spot are most likely an effect of incorrect foreground subtraction (Chiang & Naselsky 2004; Coles 2005; Liu & Zhang

2005; Tojeiro et al. 2006). This possibility has been investigated in detail for both the first year (Vielva et al. 2004; Cruz et al. 2005, 2006) and third (Cruz et al. 2007) year WMAP data. The arguments *against* foreground subtraction errors can be summarized in three main points – 1) The region of the spot shows no spectral dependence in the WMAP data. This is consistent with the CMB and inconsistent with the known spectral behavior of galactic emission (as well as the SZ effect). The flat (CMB-like) spectrum is found both in temperature and kurtosis, as well as in real and wavelet space. 2) Foreground emission is found to be low in the region of the spot, making it unlikely that an over-subtraction could produce an apparent non-Gaussianity. 3) Similar results are found when using totally independent methods to model and subtract out the foreground emission (Cruz et al. 2006), namely the combined and foreground cleaned Q-V-W map (Bennett et al. 2003) and the weighted internal linear combination analysis (Tegmark et al. 2003).

In light of our findings, we can ask whether a 20-30% decrement in the local extragalactic synchrotron emission could translate into a foreground subtraction problem that could generate the WMAP cold spot. We are not re-examining the foreground question *ab initio*, simply examining the plausibility that the deficit of NVSS sources could complicate the foreground calculations in this location. The characteristic brightness in the 3.4° convolved NVSS image around the cold spot is ~ 51 mK at 1.4 GHz; the brightness of the cold spot is ~ 37 mK. This difference of 14 mK in brightness (4 mK at 10° resolution) represents the extragalactic population contribution only, as the NVSS is not sensitive to the large scale galactic synchrotron emission. By contrast, the single dish 21 cm brightness within a few degrees of the cold spot is ~ 3.4 K, as measured using the Bonn Stockert 25 m telescope (Reich and Reich 1986). This implies a synchrotron contribution of ~ 0.7 K above the CMB, 50 times larger than the extragalactic deficit.

One way to create the cold spot would be if the universal spectral index used for the normal galactic (plus small extragalactic) subtraction was incorrect for the extra brightness temperature contribution of the NVSS dip, δT (-14 mK at L band, 21 cm). We make an order of magnitude estimate of this potential error. Following the first year data analysis (Bennett et al. 2003) (and the similar exercise performed by Cruz et al. (2006)), we consider fitting a synchrotron template map at some reference frequency ν_{ref} , and extrapolating the model with a spectral index of $\beta = -3$ to the Q, V, and W bands. This spectral index is consistent with those of Cruz et al. (2006) and the average spectral index observed in the WMAP images (Bennett et al. 2003; Hinshaw et al. 2006). Making the assumption that the spectral index of δT is the same as that of the mean brightness T_0 , we then calculate in the region of the deficit,

$$F(\nu)_{model} = [T_0(\nu_{ref}) + \delta T(\nu_{ref})] (\nu/\nu_{ref})^{-3}. \quad (1)$$

However, if the actual spectrum of δT is $-\alpha$ (from L band through W band) instead of -3, then the true foreground subtraction, $F(\nu)_{true}$, should have been

$$F(\nu)_{true} = T_0(\nu_{ref}) (\nu/\nu_{ref})^{-3} + \delta T(\nu_{ref}) (\nu/\nu_{ref})^{-\alpha}. \quad (2)$$

The foreground subtraction would then be in error as a function of frequency as follows, expressed in terms of the L band temperatures :

$$\delta F(\nu) = \delta T(\nu_L) (\nu_L/\nu)^\alpha [1 - (\nu_{ref}/\nu)^{3-\alpha}]. \quad (3)$$

Three different reference frequencies have been used for synchrotron extrapolation – the Haslam et al. (1981) 408 MHz map (Bennett et al. 2003), the Jonas, Baart & Nicolson (1998) 2326 MHz Rhodes/HartRAO survey (Cruz et al. 2006), and the internal K and Ka band WMAP images (Hinshaw et al. 2006). Since the foreground subtraction errors would be worst extrapolating from the lowest frequency template, we look at the problems from a dip spectral index that is different than -3 starting at 408 MHz. We have obtained a rough measure of the spectral index of the dip by comparing the 1° resolution maps (Figure 2) at 408 MHz and 1400 MHz. At $l_{II}, b_{II} = 207^\circ, -55^\circ$, we find $\delta T = 2.6 \pm 0.75$ K (30 ± 12 mK) at 408 (1400) MHz, yielding a spectral index of -3.6 ± 0.5 . Nominally, this would actually lead to a “hot spot” if a spectral index of -3.0 had been assumed for the extrapolation. Within the errors, the worst foreground extrapolation mistakes would then range from -0.5 to $+4.6 \mu\text{K}$ at Q band, and would go down by another factor of two at 4° resolution. In any case, this is far below the $-73 \mu\text{K}$ observed, and we thus conclude that the deficit of NVSS sources does not lead to a significant foreground subtraction error of either sign.

4. Discussion

The WMAP cold spot could have three origins: at the last scattering surface ($z \sim 1000$), cosmologically local ($z < 1$), or galactic. Because the spot corresponds to a significant deficit of flux (and source number counts) in the NVSS, we have argued here that the spot is cosmologically local and hence, a localized manifestation of the late ISW effect.

Cruz et al. (2005, 2007) derived a temperature deviation for the cold spot of $\sim -20 \mu\text{K}$ and a diameter of 10° using the WMAP 3 year data; on scales of 4° the average temperature is

lower, $\sim -73 \mu\text{K}$. Using these two data points we derive an approximate relation between the temperature deviation and the corresponding size of the cold spot: $\theta(\Delta T/T) \approx 4.5 \times 10^{-5}$, where θ is the radius of the cold spot in degrees. We now perform an order of magnitude calculation to see if the late ISW can produce such a spot, assuming that the entire effect comes from the ISW.

The contribution of the late ISW along a given line of sight is given by $(\Delta T/T)|_{ISW} = -2 \int \dot{\Phi} d\eta$, where the dot represents differentiation with respect to the conformal time η , $d\eta = dt/a(t)$, and a is the scale factor. The integrand will be non-zero only at late times ($z < 1$) when the cosmological constant becomes dynamically dominant.

We start with the Newtonian potential given by

$$\Phi = GM/r \approx \frac{4\pi G}{3} r^2 \rho_b \delta. \quad (4)$$

The proper size r and the background density ρ_b scale as a and a^{-3} , respectively. The growth of the fractional density excess, $\delta(a)$ in the linear regime is given by $D(a) = \delta(a)/\delta(a_0)$, and $D(a)$ is the linear growth factor. For redshifts below ~ 1 in ΛCDM , this factor can be approximated as $\delta(a) \approx a\delta(a_0)(3-a)/2$. Assuming that the region is spherical, its comoving radius is $r_c = 0.5\Delta z(c/H)$, and Δz is the line of sight diameter of the region. The change in the potential over $d\eta$ can be approximated by

$$\Delta\Phi \sim \frac{4\pi G}{3} r_c^2 \rho_c \delta(\Delta z), \quad (5)$$

where subscript c refers to the average comoving size of the void and the comoving background density. In ΛCDM the Hubble parameter is roughly given by $H^2 = H_0^2(1+2z)$, for redshifts below ~ 1 . Incorporating these approximations we get the following relation between the size of the region, its redshift and the temperature deviation from the late ISW:

$$\Delta\Phi \approx -\frac{\Omega_m}{4} \left(\frac{r_c}{c/H_0} \right)^3 (1+2z)^{1/2} \delta \approx \frac{1}{2} \frac{\Delta T}{T} \quad (6)$$

We now ask under what conditions this expression is consistent with the observed relation between the size and temperature of the cold spot derived earlier, $\theta(\Delta T/T) \approx 4.5 \times 10^{-5}$. For $\Omega_m \sim 0.3$ and $\delta = -1$ (i.e. a completely empty region) this leads to the simplified relation, $\theta(1+z) \approx 0.1$. Since the spot's association with the NVSS places it at $z \sim 0.5 - 1$, this leads to a self-consistent value of the radius of $\sim 3^\circ$ for the observed spot. For $c/H_0 = 4000 \text{ Mpc}$, the comoving radius of the void region is 140 Mpc.

How likely is such a large underdense region in a concordance cosmology? Suppose there is only one such large underdense region in the whole volume up to $z=1$. The corresponding void frequency is then the ratio of the comoving volume of the void to the comoving

volume of the Universe to $z=1$, which is roughly 3×10^{-5} . Is this consistent with Λ CDM? Void statistics have been done for a number of optical galaxy surveys, as well as numerical structure formation simulations. Taking the most optimistic void statistics (filled dots in Fig. 9 of Hoyle & Vogeley, 2004) which can be approximated by $\log P = -(r/\text{Mpc})/15$, a 140 Mpc void would occur with a probability of 5×10^{-10} , considerably more rare than our estimate for our Universe (3×10^{-5}) based on the existence of the cold spot. One must keep in mind, however, that observational and numerical void probability studies are limited to $r_c \sim 30$ Mpc; it is not yet clear how these should be extrapolated to 140 Mpc.

The need for an extraordinarily large void to explain the cold spot, now that we know it is a local cosmological effect, adds to the list of anomalies associated with the CMB. These include the systematically higher strength of the late ISW correlation measured for a variety of mass tracers, compared to the WMAP predictions (see Fig. 11 of Giannantonio et al. 2006), and the alignment and planarity of the quadrupole and the octopole (de Oliveira-Costa et al. 2004; Land & Magueijo 2005). We can, however, conclude that models linking the cold spot with the larger scale anomalies, such as the anisotropic Bianchi Type VII_h model of Jaffe et al. (2005), are no longer necessary. The cold spot is now seen to be a local effect, while low order global anisotropic models (e.g., Gumrukcuoglu, Contaldi & Peloso 2006) may still be needed for the low- ℓ anomalies.

5. Concluding Remarks

We have detected a significant dip in the average surface brightness and number counts of radio sources from the NVSS survey at 1.4 GHz in the direction of the WMAP cold spot, ruling out both statistical coincidence and instrumental artifacts due to foreground subtraction. It is also seen in an independent wavelet analysis and in an independent map at 408 MHz. The cold spot therefore arises from effects along the line of sight, and not at the last scattering surface itself. Any non-gaussianity of the spot therefore has a local origin.

A 140 Mpc radius, completely empty void at $z \leq 1$ is sufficient to create the magnitude and size of the cold spot through the late integrated Sachs-Wolfe effect. Voids this large currently seem improbable in the concordance cosmology, adding to the anomalies associated with the CMB.

We suggest that a closer investigation of all mass tracers would be useful to search for significant contributions from isolated regions. Also, if our interpretation of the cold spot is correct, it might be possible to detect it indirectly using Planck, through the lack of lensing-induced polarization B modes (Zaldarriaga & Seljak 1997).

ACKNOWLEDGMENTS We thank Eric Greisen, NRAO, for improvements in the AIPS FLATN routine, which allows us to easily stitch together many fields in a flexible coordinate system. The 408 MHz maps were obtained through *SkyView*, operated under the auspices of NASA’s Goddard Space Flight Center. We appreciate discussions with M. Peloso, T. J. Jones and E. Greisen regarding this work. LR acknowledges the inspiration from his thesis adviser, the late David T. Wilkinson, who would have appreciated the notion of deriving information from a hole. At the University of Minnesota, this work is supported in part, through National Science Foundation grants AST 03-07604 and AST 06-07674 and STScI grant AR-10985.

REFERENCES

- Bennett, C.L., et al. 2003, ApJS 148, 1
- Cabre, A., Gaztanaga, E., Manera, M., Fosalba, P. Castander, F. 2006, MNRAS 372, 23
- Cayon, L., Jin J., Treaster, A. 2005, MNRAS 362, 826
- Chiang, L.-Y., Naselsky, P.D. 2006, IJMPD 15,1283C
- Coles, P. 2005, Nature 433, 248
- Condon, J. J., Cotton, W. D., Greisen, E. W., Yin, Q. F., Perley, R. A., Taylor, G. B., Broderick, J. J. 1998, AJ 115, 1693
- Crittenden, R. G., Turok, N. 1996, PRL 76, 575
- Cruz, M., Martinez-Gonzalez, E., Vielva, P., Cayon, L. 2005, MNRAS 356, 29
- Cruz, M., Tucci, M., Martinez-Gonzalez, E., Vielva, P. 2006, MNRAS 369, 57
- Cruz, M., Cayon, L., Martinez-Gonzalez, E., Vielva, P., Jin, J. 2007, ApJ 655, 11
- de Oliveira-Costa A., et al. 2004, PhRevD 69, 3516
- Giannantonio, T. et al. 2006, PhRvD 74, 352
- Gumrukcuoglu, A. E., Contaldi, C. R. & Peloso, M. 2006, astro-ph/0608405
- Haslam, C. G. T., Klein, U., Salter, C. J., Stoffel, H., Wilson, W.E., Cleary, M.N., Cooke, D.J., & Thomasson, P. 1981, A&A, 100,209
- Hinshaw, G., et al. 2006, ApJ, submitted (astro-ph/0603451)

- Hoyle, F., Vogeley, M. S. 2004, ApJ 607, 751
- Jaffe, T. R., Banday A. J., Eriksen, H. K., Forski, K. M, Hansen, F. K. 2005, ApJ 629, L1
- Jonas, J., Baart, E. E., Necolson, G. D. 1998, MNRAS, 297, 997
- Land, K., Magueijo, J., 2005, PRL 95, 071301
- Liu, X., & Zhang, S. N. 2005, ApJ, 633, 542
- McEwen, J. D., Vielva, P., Hobson, M. P., Martinez-Gonzalez, E., & Lasenby, A. N. 2007, MNRAS, in press
- Pietrobon, D., Balbi, A., Marinucci, D. 2006, PhysRevD 74, 352
- Reich, W. and Reich, P. 1986, A&A Suppl. 63, 205
- Tegmark, M., de Oliveira-Costa, A., Hamilton A. 2003, Phys.Rev. D68, 123523.
- Tojeiro, R., Castro, P.G., Heavens, A.G., Gupta, S. 2006, MNRAS, 365, 265
- Vielva, P., Martinez-Gonzalez, E., Varreiro, R. B., Sanz, J. L., Cayon, L. 2004, ApJ 609, 22
- York, D. G. et al. 2000, AJ 120, 1579
- Zaldarriaga, M. & Seljak, U. 1997, PhRvD 55, 1830

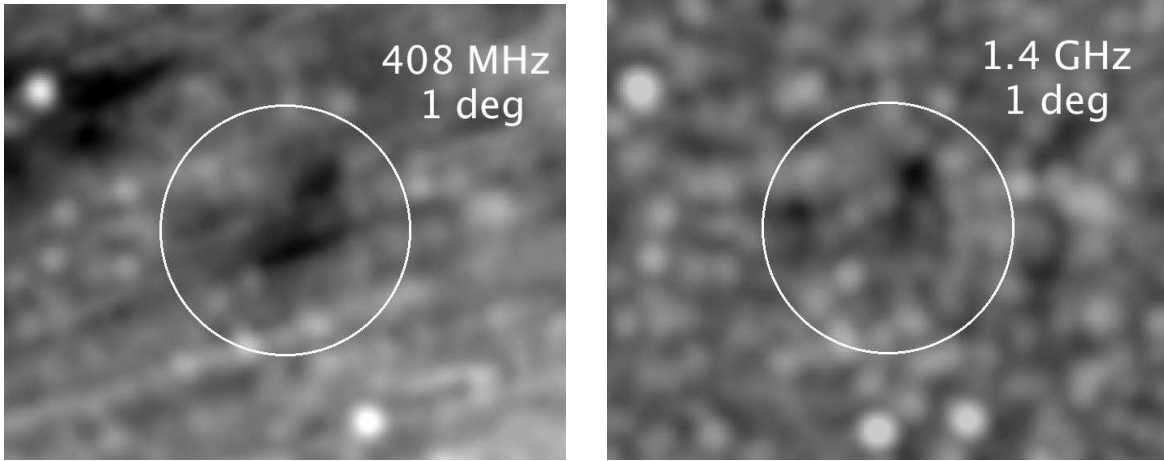


Fig. 1.— 18° fields, with 1° resolution, centered at $l_{II}, b_{II} = 209^\circ, -57^\circ$. Left: 408 MHz (Haslam et al. 1981). Right: 1.4 GHz (Condon et al. 1998). A 10° diameter circle indicates the position and size of the WMAP cold spot.

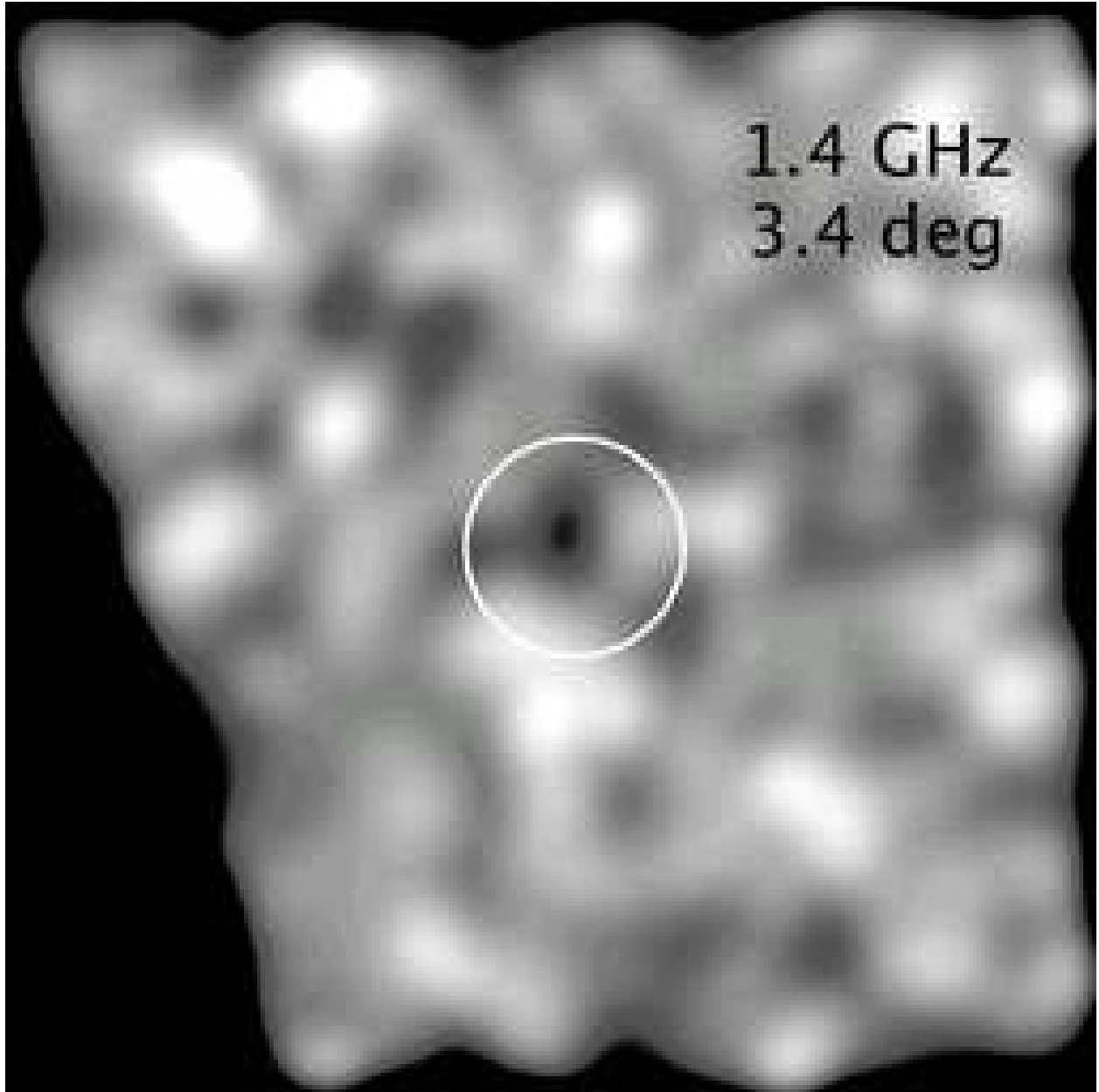


Fig. 2.— 50° field from smoothed NVSS survey at 3.4° resolution, centered at l_{II} , b_{II} = 209°, -57°. A 10° diameter circle indicates the position and size of the WMAP cold spot.

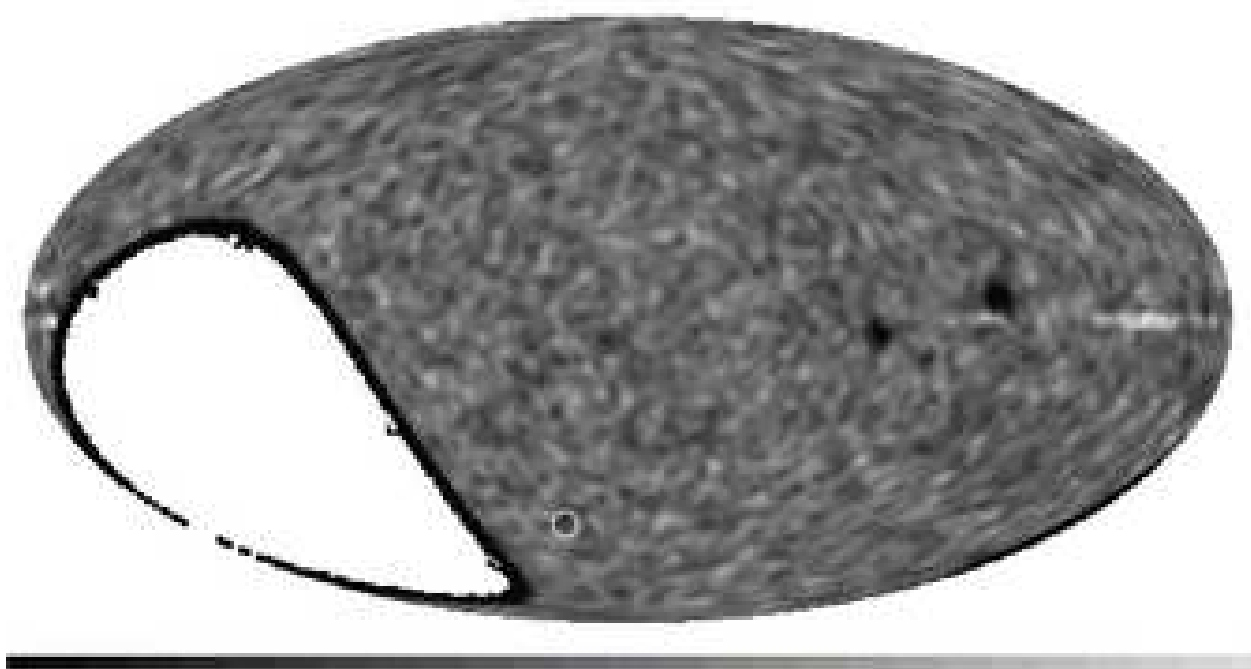


Fig. 3.— Aitoff projection of NVSS survey, centered at l_{II} , $b_{II} = 180^\circ$, 0° , showing the median brightness in sliding boxes of 3.4° . The WMAP cold spot is indicated by the white circle. Near the plane, large dark patches arise from sidelobes around strong NVSS sources.

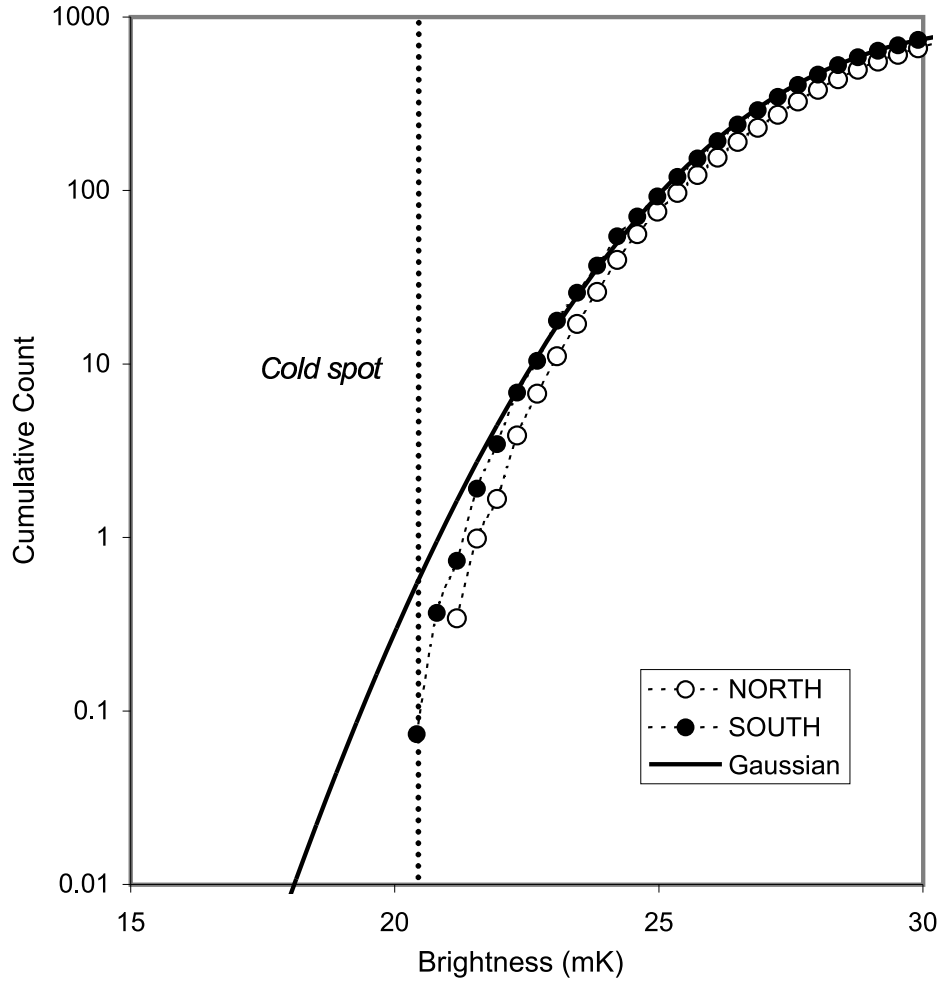


Fig. 4.— The cumulative distribution, normalized to 1000, of median brightness levels in 3.4° sliding boxes of the NVSS images in two strips above $|b_{II}| > 30^\circ$ (see text). The minimum brightness (equal to the cold spot region) is indicated by a vertical line. A Gaussian distribution is shown as a solid line for comparison.

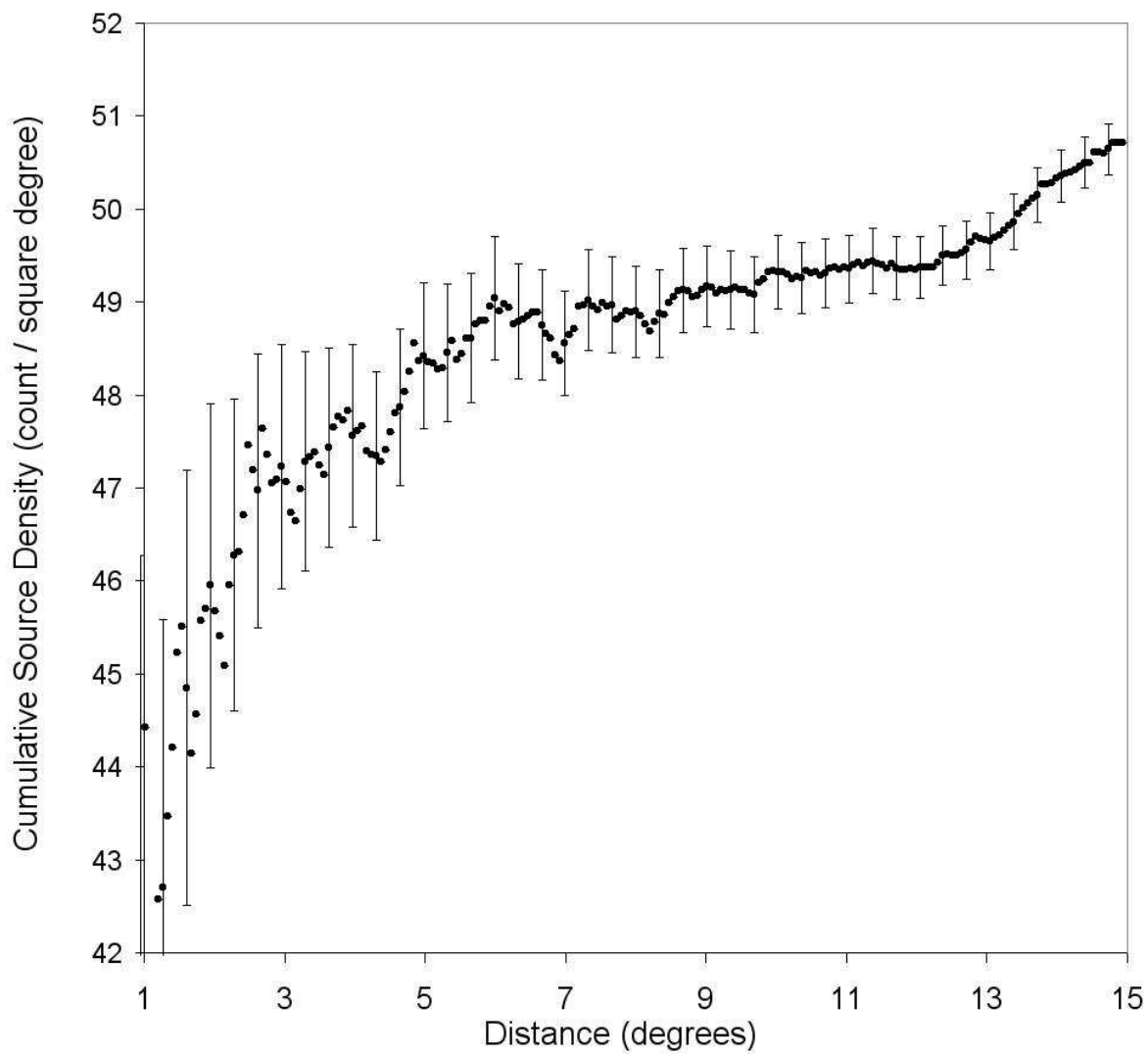


Fig. 5.— Cumulative number per unit area of NVSS sources above 1.5 mJy/(45'' beam) as a function of distance from the WMAP cold spot. Error bars reflect counting statistics, but are not independent.